Ultramicroscopy 281 (2026) 114297

Contents lists available at ScienceDirect

Ultramicroscopy

journal homepage: www.elsevier.com/locate/ultramic

Basic considerations in the design of an electrostatic electron monochromator

M.J. Adriaans *, J.P. Hoogenboom, A. Mohammadi-Gheidari *

Department of Imaging Physics, Delft University of Technology, Delft, the Netherlands

ARTICLE INFO

Keywords:
Electrostatic monochromator
Fringe-field deflector
MEMS fabrication
Low-voltage SEM (LVSEM)
Energy Filtering
Electron optics

ABSTRACT

Monochromators are essential components in electron microscopy and spectroscopy for improving spatial and energy resolution. Their use in scanning electron microscopes (SEMs), however, remains limited due to high cost and operational complexity. Using a thin-deflector analysis of a homogeneous electrostatic deflector, we show that conventional monochromators exhibit extreme sensitivity to power-supply drift and mechanical imperfections. Meeting these stringent tolerances typically requires additional correction elements, which further increase system complexity and cost.

We demonstrate that fringe-field deflectors are inherently less sensitive to these limitations. Based on this insight, we propose a simple and cost-effective monochromator architecture relying solely on fringe fields. The design achieves optimal energy resolution by incorporating short-range deceleration lenses surrounding the main deflector, eliminating the need for auxiliary correction elements. Such a fully electrostatic configuration is compatible with MEMS fabrication, offering a compact, robust, and accessible pathway for high-performance energy filtering in SEMs.

1. Introduction

In recent years, there has been growing interest in Low-Voltage Electron Microscopy (LVEM), particularly Low-Voltage Scanning Electron Microscopy (LVSEM), for applications such as imaging the surface of charging sample [1,2]. However, as the beam energy decreases, chromatic aberration blur significantly degrades the resolution, especially at extremely low landing energies, in the range of only a few hundred electron-volts (eV). Reducing the energy spread of the electron source greatly mitigates this issue, as illustrated in Fig. 1a. The figure shows the variation of the axial FW50 probe diameter, d_p, which contains 50 % of the total probe current as a function of the beam opening angle, α. To calculate d_p different contributions are added according to [3]:

$$d_p = \left(\left[d_{geo}^{1.3} + \left(d_\lambda^4 + d_s^4 \right)^{\frac{1.3}{4}} \right]^{\frac{2}{1.3}} + d_c^2 \right)^{\frac{1}{2}} \quad (1)$$

where $d_{geo} = \frac{2}{\pi}\sqrt{\frac{I}{B_r \phi}}\ \frac{1}{\alpha}$ is the FW50 size of the geometric source image, $d_c = 0.6 C_c \frac{dE}{E}\alpha$ is the FW50 size of the chromatic aberration blur, $d_s = 0.18 C_s \alpha^3$ is the FW50 size of the spherical aberration blur and $d_\lambda = 0.54 \frac{\lambda}{\alpha}$ is the FW50 size of the diffraction blur. In these expressions, B_r is the reduced brightness of the electron source, ϕ is the acceleration potential ($E = e\phi$= acceleration energy), dE is the (FW50) energy spread of the electron source, λ is the wavelength of the electrons, C_s and C_c are the spherical and chromatic aberration coefficients of the objective lens, respectively.

As demonstrated in Fig. 1a, reducing the energy spread dE, for example, by incorporating a monochromator, improves the spatial resolution of LVSEM's. Monochromators are widely used in High-Resolution-Electron-Energy-Loss-Spectroscopy (EELS) to enhance energy resolution and in (Scanning) Transmission Electron Microscope ((S)TEM) to improve spatial resolution [4]. However, this is not particularly the case for SEM's, mainly due to the higher cost and complexity of current monochromator designs.

Several monochromator concepts exist for (S)TEM and EELS, such as the Alpha-, Omega-, and Wien-type monochromators [4,5]. Their underlying electron-optics working principles are schematically illustrated in Fig. 2. At the core of all these designs lies a "uniform" magnetostatic field or electrostatic field, or a combination of both, which produces angular dispersion of the beam.

* Corresponding authors.
E-mail addresses: m.adriaans@tudelft.nl (M.J. Adriaans), a.m.gheidari@tudelft.nl (A. Mohammadi-Gheidari).

https://doi.org/10.1016/j.ultramic.2025.114297
Received 27 January 2025; Received in revised form 2 December 2025; Accepted 6 December 2025
Available online 9 December 2025

The performance of a monochromator is typically evaluated by its theoretical energy resolution. Although this seems a natural metric, relying on this number alone is misleading. One should also consider the cost and operational complexity of the system. In practice, monochromators are far more complicated than the simple dispersive elements shown schematically. The grey-dotted regions in Fig. 2 represent additional correction elements, usually multipoles, required to compensate for mechanical imperfections and to correct geometric aberrations. Almost all high-performance monochromators include such complex and expensive correction modules. Consequently, the cost and complexity of current monochromators largely depend on the level of correction optics added to the original theoretical design.

Because of these factors, monochromators are rarely used in SEM columns. To the best of our knowledge, only one commercially available monochromator concept exists for SEMs, the UC gun [6]. Unlike the previously mentioned designs, the UC concept relies on a relatively simple modification of the electron gun and achieves an energy resolution of ~150 meV. For LVSEM applications, a monochromator offering a better energy resolution together with reduced cost and complexity is therefore highly desirable.

The aim of this paper is to explore why and how current monochromators are so expensive and complex. In Sections 2 and 3, the main parameters influencing the dispersion resolution of the dispersive element, assumed here, for simplicity and without loss of generality, to be a simple electrostatic deflector, are analysed and their boundaries are discussed. In Section 4, a basic layout for a simple monochromator, free from these limitations and specifically designed for LVSEM, is proposed.

2. Requirements for an electrostatic-deflector-based monochromator

In a simplified monochromator based on a single dispersion element, here, an electrostatic deflector, a (semi-)collimated beam traversing through the system experiences angular dispersion. This dispersion is then imaged onto a selection aperture or slit plane. The corresponding schematic layout is shown in Fig. 3. Although the figure depicts a straight- axis deflector, the results are, to some extent, also applicable to other geometries, such as a curved-axis deflector schematically shown in Fig. 2.

In a deflector, the deflection angle θ is a function of acceleration potential ϕ. A kinetic energy spread dE, Expressed here in terms of $d\phi = \frac{dE}{e}$ (with elementary charge e), causes a spread in the deflection angle, $d\theta$ due to transverse chromatic aberration. A linear expansion of the transverse electrostatic deflection angle around ϕ yields:

$$\frac{d\phi}{\phi} = -\frac{d\theta}{\theta} \tag{2}$$

This angular spread of electrons with different energies passing through a deflector is the key characteristic of deflector-based monochromators. To select a specific energy window, a lens positioned at the exit plane of the deflector converts this angular dispersion into spatial dispersion.

In the dispersion plane, a slit selects the desired energy window and blocks the remainder of the energy spectrum.

An ideal monochromator should provide a large dispersion to enable selection of a narrow energy window. To optimize the energy resolution, the slit size is chosen to match the size of the focused probe of electrons with nominal beam energy. Ideally, the probe size at the slit plane should be equal to the geometric image of the source at that plane. However, this is not generally the case. The probe is typically larger than the geometric image of the source due to additional contributions, thereby degrading the energy resolution of the monochromator. Here, we investigate the main parameters that affect the energy resolution of a monochromator. Specifically, we focus on the performance-limiting parameters of the main dispersive element, the deflector. Furthermore, we restrict our analysis to the uncompensated case, where no additional correction is applied for the inherent limitations of deflector-based monochromators as considered here. To isolate the contributions of the main deflector alone, we study the impact of various parameters that influence the smallest discernible angle, $d\theta$, at the deflector exit plane.

An analytical description of thin deflectors and the geometric aberration contribution to the smallest discernible angle is presented in subSection 2.1. These results are then used to derive the effect of electric potential instabilities in subSection 2.2. In SubSection 2.3, we discuss the contributions from mechanical misalignments and finally, the effect of Coulomb interaction is analysed in SubSection 2.4.

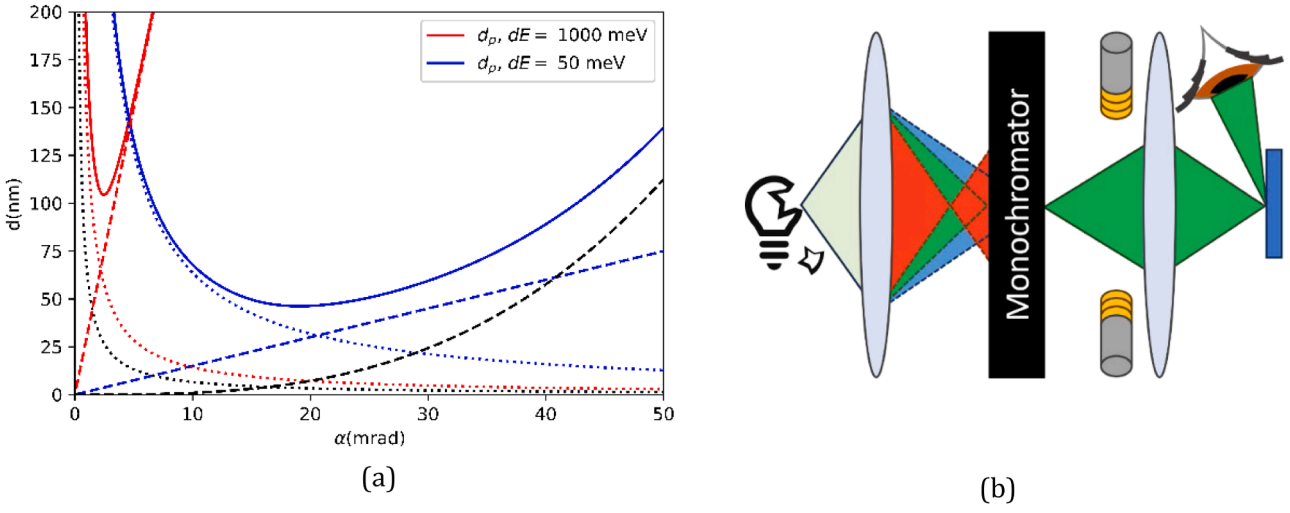

Fig. 1. (a) FW50 probe size for different dE (red for 1000 meV and blue for 50 meV) due to a combination of geometric spot size (decreasing dotted-red and -blue curves) and chromatic aberration (increasing dashed-red and -blue curves), diffraction (decreasing dotted black curve) and spherical aberration (increasing dashed black curve) leading to a combined total spot size indicated by the unbroken red and blue lines. Here we take $C_s = C_c = 5$ mm, (fixed) probe current of 0.5 nA and an acceleration energy, $E = 100$ eV. (b) Schematic illustration of a monochromated SEM column. The source (depicted as a broken light bulb) emits an unfiltered electron beam and in a first crossover the spot is blurred due to the chromatic aberration of the first illustrated lens. A (schematically illustrated) black box monochromator removes the electrons with higher (blue) and lower (red) kinetic energies than the nominal (green) electron beam energy. The filtered beam is then focused onto a sample plane.

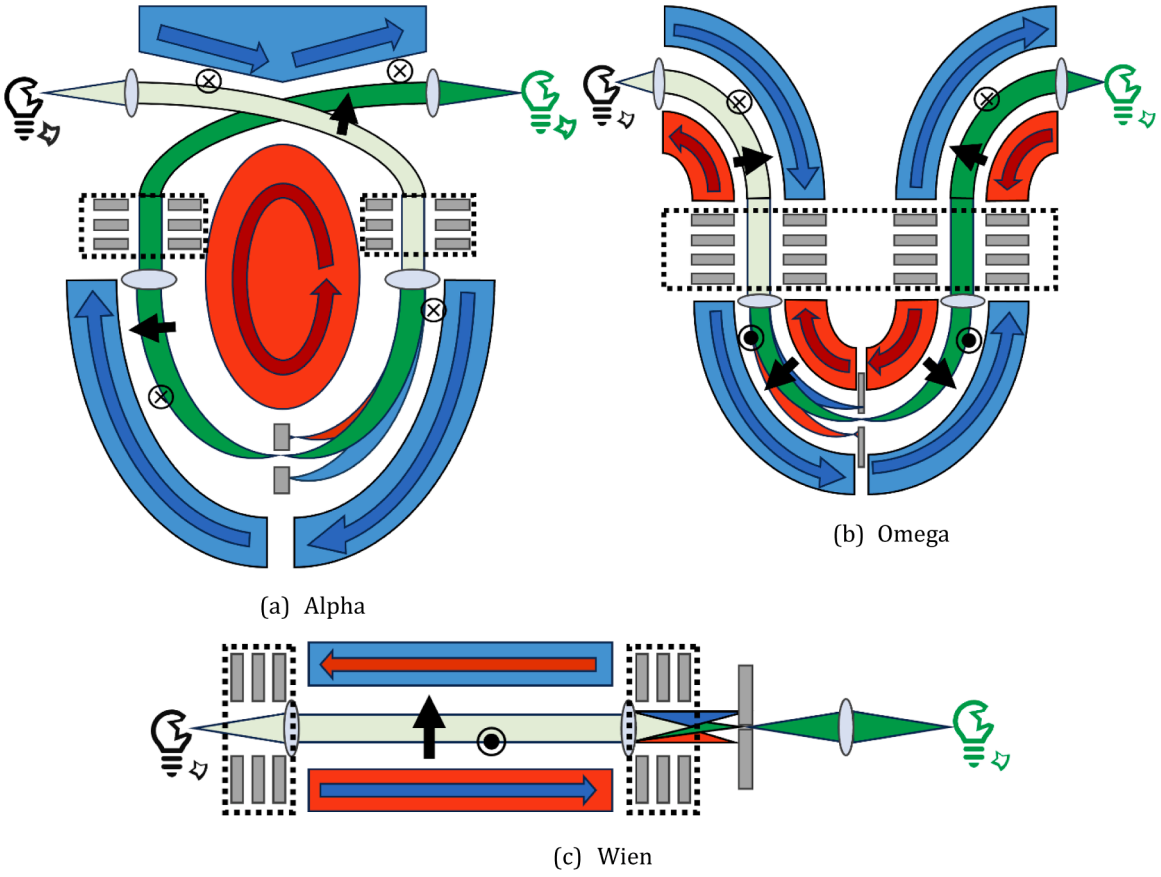

Fig. 2. Schematic illustration of the electron optics working principle of current monochromator layouts. (a) Alpha type, (b) Omega type, and (c) Wien type monochromators. The Alpha and Omega designs can be implemented using either magnetostatic or electrostatic fields. In the magnetostatic configuration, the red and blue arrows indicate the direction of the currents in the surrounding coils or conductors, which generate the magnetic field responsible for beam curvature. In the electrostatic implementation, an applied voltage difference produces an equivalent deflection. In the Wien type monochromator, crossed magnetostatic and electrostatic fields create energy dispersion, where electrons with the nominal beam energy remain undeflected.

2.1. Geometric aberrations

The deflection of a collimated electron beam in a thin deflector is schematically illustrated in Fig. 3. The collimated beam enters and exits a deflector at an angle $\theta/2$, maintaining a constant x-coordinate throughout the deflection region.[1] The internal beam angle, α, is defined as the ratio between the effective focal length of the collimating lens and the (virtual) source radius, r_s. The beam radius, r, is assumed to remain constant throughout the deflector.

The deflection region is modelled as a homogeneous deflection field with a sharp cutoff. This assumption implies that electrons are accelerated in the z-direction only upon entering and leaving the deflector. The fringe-field effect in the x-direction is negligible compared to the main deflection caused by the homogeneous field, provided the deflector is narrow and weakly excited.

Therefore, the effect of the fringe-field shape of on the monochromator resolution is neglected. The change in the (non-relativistic) momentum, $\vec{v}$, of an electron with velocity $\vec{v}$ due to the Lorentz force, is given by

$$\frac{1}{m}\frac{d\vec{p}}{dt} = \frac{d\vec{v}}{ds}v = \frac{e}{m}\vec{\nabla}\phi, \tag{3}$$

where ϕ is the electrostatic potential, e the elementary charge, m the electron (rest-)mass, and ds an infinitesimal path element along the electron trajectory. Fixing the ground potential as $e\phi = \frac{1}{2}mv^2$, and

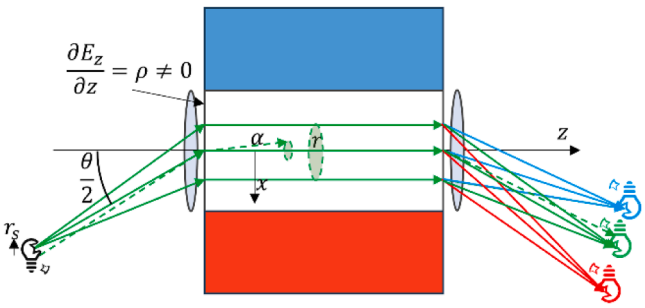

Fig. 3. Schematic representation of the thin-deflector approximation. The beam enters at an angle; the transverse x-position of electron is assumed to remain constant throughout the deflector, and electron leaves the deflector with the same initial angle but in the opposite direction. The lenses are includede to illustrate positional dispersion. In practice, They also introduce chromatic defocus, shown here as different focal planes for the red and blue rays. The dashed green line indicates that the beam angle **α** is equal to the ratio between the (virtual) source radius and the effective focal length **r_s/f**, respectively. The effect of this angle is exagerrated for clarity in the schematic. The radius of the collimated beam is **r**.

[1] Typically, the constant ϕ before the deflector is equal to the constant ϕ after the deflector. Integration over a straight axis $x = x_0$ always yields $\Delta v_z = 0$ for systems with middle symmetry. This makes $v_{x,0} = -v_{x,1}$ (before and after deflector). This, in turn, implies that a blurred focused spot behind the deflector is caused by an equally blurred incoming beam before the deflector. This is a valid assumption as long as the size of the blurred spot is smaller than the collimated beam radius.

integrating over a known trajectory s, yields

$$\Delta\vec{v} = \eta \int \vec{\nabla}\phi^{\frac{1}{2}} ds \tag{5}$$

[2]with $\eta = \sqrt{\frac{2e}{m}}$.

For a homogeneous-field deflector, the exact trajectory s is a parabola, and we can expand around the initial coordinates to obtain the aberrations, as done previously [7]. In this formulation, any assumed (trial) trajectory, including a parabolic one, can be substituted to obtain an approximate result.

To keep this approach simple for generalized forms of ϕ, we approximate $ds \approx dz$, assuming that the electron travels at a constant x-position (the thin-deflector approximation) through the deflector. The trajectory is schematically illustrated in Fig. 3.

Dividing Δv_x by the velocity far from the deflector, $v_0 = \eta\sqrt{\phi_0}$, where the potential is constant (ϕ_0), yields the deflection angle $\theta \approx 2\sin\left(\frac{\theta}{2}\right) = \frac{\Delta v_x}{v_0}$ (small-angle approximation), thus

$$\theta = \frac{1}{\sqrt{\phi_0}} \int \frac{\partial}{\partial x}\phi^{\frac{1}{2}} dz. \tag{6}$$

This then allows a Taylor expansions of x-component of the integrand with respect to x as

$$\theta = \frac{1}{\sqrt{\phi_0}} \int dz \left[O(x^3) + \frac{\phi'(0)}{2\phi(0)^{\frac{1}{2}}} + x\frac{2\phi(0)\phi(0) - \phi'(0)^2}{4\phi(0)^{\frac{3}{2}}} + x^2\frac{4\phi(0)^2\phi'''(0) + 3\phi'(0)^3 - 6\phi(0)\phi'(0)\phi''(0)}{16\phi(0)^{\frac{5}{2}}} \right] \tag{7}$$

In this expansion, the first term (x^0) represents the deflection effect of the deflector. The second term (x^1) corresponds to the astigmatic focusing effect, and the third term (x^2) represents the second-order aberration, which is a comatic term.[3] This comatic aberration distorts the spot shape into a comet-like and trefoil blur, thereby limiting the smallest discernible angle. For a homogeneous deflection field, as considered here, only the $\phi'(0)^3$ term contributes to the x^2 aberration, while the effects of other terms vanish. However, this is not necessarily the case for other monochromator designs. For instance, in the UC, where the beam traverses off-axis through a lens with spherical aberrations, $\phi'''(0) \neq 0$. A recent approach to mitigate this issue involves using an off-axis microlens [8].

The potential of a homogenous deflector can be written as:

$$\phi = \phi_0 + \frac{\Delta\phi}{D}x \tag{8}$$

Where $\Delta\phi$ is the potential difference across an ideal deflector with an electrode separation D. Substituting Eq. (8) into Eq. (7)and integrating over the deflector length L yields:

$$\theta = \frac{L\Delta\phi}{2D\phi_0} - \frac{xL}{4D^2}\left(\frac{\Delta\phi}{\phi_0}\right)^2 + \frac{x^2L}{D^3}\left(\frac{3\Delta\phi^3}{16\phi_0^3}\right) \tag{9}$$

$$= \theta_0 - \left(\frac{x}{L}\right)\theta_0^2 + \frac{3}{2}\left(\frac{x}{L}\right)^2\theta_0^3 \tag{10}$$

where $\theta_0 = \frac{L\Delta\phi}{2D\phi_0}$. Similar to how d_s degrades the smallest discernible probe size d_p in a focussed probe (see Eq. (1)), the angular comatic term here causes a deterioration of the angular resolution, $d\alpha_{Co}$, given by

$$d\alpha_{Co} \approx \frac{3}{2}\left(\frac{r}{L}\right)^2\theta_0^3, \tag{11}$$

where, r is the beam radius.

2.2. Power supply instability

The inverse time-of-flight of electrons in a monochromator is much higher than the bandwidth of any electrostatic power supply connected to the electrodes. For instance, even in an LVSEM operating at $\phi_0 \leq 1$ kV, electrons traverse the column at 2×10^7m/s. This means that, for a column length of one meter, any interference slower than 2×10^7 Hz can be considered a static drift. Although small drifts can cause the dispersed beam to shift relative to the energy-selection slit, the instantaneous energy resolution for any electron wave packet entering the monochromator is not affected by temporal fluctuations in the electric field. However, such drifts do cause the nominal pass energy of the monochromator to vary over time. In EELS, the issue is less pronounced, since the deflector supplies of both the monochromator and analyser can be synchronously linked to compensate symmetrically for the nominal energy drift [9].

For LVSEM imaging, however, the time-averaged energy resolution, integrated over the acquisition time per image, serves as a measure of the practical energy resolution. Monochromators typically achieve energy resolutions close to their theoretical specifications only for milliseconds or less, relying on power supplies with relative accuracies on the order of a few parts per billion [10]. The sensitivity monochromator deflectors to voltage fluctuations, which affect the deflection angle θ, can be found by expanding around $\Delta\phi$, yielding the angular spread due to voltage fluctuations, $d\alpha_s$, as

$$d\alpha_s = \frac{L}{2D\phi_0}\delta\phi = \theta_0\frac{\delta\phi}{\Delta\phi} \tag{12}$$

From this intermediate result, we can already conclude that, for $d\phi$ to be minimally dependent on $\Delta\phi$ (i.e. for a small $d\alpha_s$), $\Delta\phi$ should be made as large as possible to minimize drifts in the deflection angle. This can be achieved by reducing the ratio L/D as much as possible.

2.3. Misalignments

Misalignments of the deflector electrodes result in parasitic aberrations that degrade the energy resolution in the absence of additional correction elements. Here, we present the effect of an antiparallel rotation of the two deflector plates relative to each other around their midpoints in the rotational z-direction, as illustrated in Fig. 4. If the deflector plates are rotated by an angle $\varphi/2$ in opposite directions about their midpoint at $y = 0$, the resulting distance D between the

[2] Equation 5 resembles the fundamental theorem of calculus in 3 dimensions: $\Delta\vec{v} = \int \vec{\nabla}v ds = \eta \int \vec{\nabla}\phi^{\frac{1}{2}} ds$ whereas, a conventional line integral is valid for any trajectory, this integral is only an approximation when ds does not follow the actual trajectory of the particle.

[3] One can correct higher order aberrations, leaving no intrinsic resolution limit due to geometric aberrations. However, a finite number of correctors will lead to a finite termination of this series expansion.

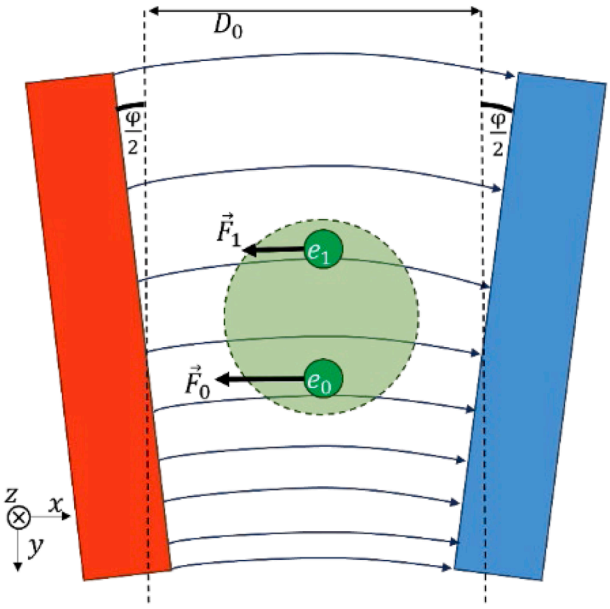

Fig. 4. The deflector plates (red and blue) are rotated antiparallel by a small angle $\frac{\varphi}{2} \ll 1$. This results in an inhomogeneous deflection force experienced by different parts of the beam (indicated by electrons $\boldsymbol{e}_0$ and $\boldsymbol{e}_1$).

electrodes is:

$$D(y) = D_0 - 2y\tan\frac{\varphi}{2} \approx D_0\left(1 - \frac{y}{D_0}\varphi\right) \tag{13}$$

Substituting this linear approximation into our expression for θ_0 yields a contribution α_φ:

$$d\alpha_\varphi := \theta_0\frac{y}{D_0}\varphi \approx \theta_0\frac{r}{D_0}\varphi \tag{14}$$

The loss of angular resolution arises from rays traversing the deflector near the edge, where $y \approx r$. The linear defects dominate initially (since φ can be made arbitrarily small to ensure this), while higher-order aberrations require more complex correction elements than the linear terms. Therefore, the mechanical tolerances for a given energy resolution are based solely on this linear effect.

2.4. Coulomb interactions

From Eq. (2), one might infer that ϕ can be arbitrarily lowered to improve the energy resolution. Although this is geometrically valid, other effects then become dominant. Assuming pencil-beam energy broadening, the Boersch effect directly adds to the energy spread of the beam as [11]:

$$d\phi_B = K\frac{m}{\epsilon_0 e^2}\frac{I^2 L}{\phi_0}. \tag{15}$$

where ε_0 is the vacuum permittivity, and $K = 0.642$ is a dimensionless constant that depends on the initial statistical distributions and cutoff criteria. Including the Boersch effect, which scales as an inverse power $\phi_0\left(i.e.,\ \frac{1}{\phi_0^n}\right)$, leads to an optimal ϕ_0 and thus a theoretical limit for the best achievable energy resolution from first principles. However, the broadening described by Eq. (15) represents an approximation valid primarily for cylindrically symmetric optics. In a monochromator, the statistical energy broadening that occurs before the deflection fields, which disperse electrons according to their energies, is irrelevant to the overall energy resolution of the system. Therefore, the relationship in Eq. (15) should be treated with caution when applied to monochromators. The topic is rich in detail for dispersive optics, and some configurations are even reported to exhibit an "inverse Boersch effect" [12], which reduces $d\phi$. Hence, further modelling of different dispersive configurations is required to accurately quantify the Boersch broadening in specific monochromator designs. Nevertheless, Eq. (15) provides a useful indication of the magnitude and scaling of statistical broadening when lowering ϕ_0 to improve $d\phi$ and is therefore used here. Unlike angular resolution losses, this effect contributes directly to the energy resolution loss in a monochromator. In addition, statistical Coulomb interactions within a monochromator can cause trajectory displacements. In the pencil-beam regime, the corresponding angular resolution loss is given by [11]:

$$d\alpha_T = \frac{C_p}{\epsilon_0}\frac{m^{\frac{3}{2}}}{e^{\frac{7}{2}}}\frac{I^3 L r}{\phi^{\frac{5}{2}}} \tag{16}$$

where $C_p = 8.31 \times 10^{-4}$. Again, there is an inverse dependence on ϕ.

3. Practical energy resolution

In the previous section, the effect of the various contributions to the angular dispersion of an electrostatic deflector were analysed. The smallest discernible angle, α_{tot}, results from the linear combination[4]

$$\alpha_{\text{tot}} = \alpha + d\alpha_{Co} + d\alpha_s + d\alpha_\varphi + d\alpha_T \tag{17}$$

which includes all sources of angular broadening. Here, α represents the current-carrying angle, whereas the other terms contribute only to the blurring of this angle. By equating α_{tot} to $d\theta$ in Eq. (2), the corresponding $d\phi$ can be obtained. Furthermore, by including the Boersch effect in $d\phi$, the total energy spread, $d\phi_{\text{tot}}$, is given as:

$$d\phi_{tot} = d\phi_\alpha + d\phi_{Co} + d\phi_s + d\phi_\varphi + d\phi_T + d\phi_B \tag{18}$$

$$= \frac{\phi}{\theta}\alpha + \frac{3}{2}\frac{I}{B_r\pi^2}\left(\frac{\theta}{\alpha L}\right)^2 + \frac{\phi}{\Delta\phi}\delta\phi + \sqrt{\frac{I\phi}{B_r\pi^2}}\frac{\varphi}{D\alpha} + \frac{C_p}{\epsilon_0}\frac{m^{\frac{3}{2}}}{e^{\frac{7}{2}}\pi}\frac{I^{\frac{7}{2}}L}{\theta\phi^2 B_r^{\frac{1}{2}}\alpha} + \frac{Km}{\epsilon_0 e^2}\frac{I^2 L}{\phi} \tag{19}$$

Here, the radius of a round beam is replaced by $r = \sqrt{\frac{I}{B_r\pi^2\alpha^2\phi}}$, where I is the unfiltered current and B_r the reduced brightness of the electron source. The indices of θ_0, ϕ_0 and D_0, as well as the negative sign of $d\phi$ have been omitted for simplicity. By differentiating this equation w.r.t α, an optimum beam angle can be found.

The Eq. (19) alone does not necessarily provide deeper insight into different individual contributions unless they are compared separately. First, we assume that the energy resolution is dominated by the geometric angle and the contribution from coma. The optimum beam angle is obtained by equating $\phi_{Co} = d\phi_\alpha$, yielding

$$\alpha = \left(\frac{3I}{2B_r\pi^2\phi L^2}\right)^{\frac{1}{3}}\theta. \tag{20}$$

Substituting this value of α into $d\phi_\alpha$ gives the optimum energy resolution in the presence of geometric and coma contributions.

$$d\phi_{\alpha,\ Co} := 2d\phi_{Co} = 2d\phi_\alpha = \left(\frac{12I\phi^2}{B_r\pi^2 L^2}\right)^{\frac{1}{3}} \tag{21}$$

Solving $d\phi_{\alpha,\ Co} = d\phi_{B,p}$ yields the optimum potential

[4] Whether a linear, RMS or another form of addition is used depends on the statistical assumptions being made. Although these methods result in different numerical values, they are mathematically equivalent in the sense that each corresponds to a specific underlying statistical distributions, information we generally do not have. Therefore, for simplicity and clarity, we adopt linear addition here.

$$\phi = IL\left(\frac{B_r\pi^2}{12}\right)^{\frac{1}{5}}\left(\frac{Km}{\epsilon_0 e^2}\right)^{\frac{3}{5}} \tag{22}$$

Substituting Eqs. (20) and (22) into Eq. (21) gives a new expression for $d\phi_{\text{tot}}$ as

$$d\phi_{\text{tot}} = d\phi_{\alpha,\text{Co,B}} + d\phi_s + d\phi_\varphi + d\phi_T \tag{23}$$

$$= 2I\left[\left(\frac{Km}{\epsilon_0 e^2}\right)^2\left(\frac{12}{B_r\pi^2}\right)\right]^{\frac{1}{5}} + \frac{\phi}{\Delta\phi}\delta\phi + \frac{\varphi L^{\frac{3}{2}} I}{D\theta 3^{\frac{1}{2}}}\left(\frac{Km}{\epsilon_0 e^2}\right)^{\frac{1}{2}} + \frac{2C_p\, m^{\frac{1}{2}} I^{\frac{3}{2}}}{\pi B_r^{\frac{3}{5}} e^{\frac{3}{2}} K\theta^2} \tag{24}$$

The first term in this equation,

$$d\phi_{\alpha,\text{Co,B}} = 2I\left[\left(\frac{Km}{\epsilon_0 e^2}\right)^2\left(\frac{12}{B_r\pi^2}\right)\right]^{\frac{1}{5}} \tag{25}$$

Is a combined effect from $d\phi_\alpha$, $d\phi_{Co}$ and $d\phi_B$. This equation represents the intrinsic energy resolution of an ideal monochromator, free from engineering imperfections such as mechanical misalignments and power-supply instabilities. The only parameters influencing this equation are those fundamentally imposed by nature. Although trajectory displacement is also an intrinsic effect, it is excluded from this expression, since, as will be shown, its contribution can be kept negligibly small.

It should be noted that, in the calculation of $d\phi_{\alpha,Co,B}$, it is assumed that

$$d\phi_{Co} = d\phi_\alpha = \frac{d\phi_B}{2}$$

This assumption gives a better energy resolution, but at the expense of a considerable practical brightness loss due to the larger contribution from coma.

For a diffraction-limited beam, the current I is replaced by the coherent current of the source, $I = 10^{-18}B_r$ [13], showing that the optimum energy resolution depends only on the reduced brightness of the source. For example, for a Schottky source with $B_r = 10^8\text{Am}^{-2}\text{V}^{-1}\text{sr}^{-1}$, hence a coherent current of 100 pA, the diffraction limited resolution is 0.1 mV. For LVSEM applications, where higher beam current (e.g., $I = 10$ nA) is typically preferred, this leads to $d\phi_{\alpha,Co,Bp} = 12$ mV.

In practice, however, this level of energy resolution is not easily achievable. This limitation arises from the three remaining terms in Eq. (24), from which a requirement can be derived for each contribution. First, the trajectory displacement is considered. By setting $d\phi_T \ll d\phi_{\alpha,Co,B}$, and rearranging the terms, we obtain

$$\theta \gg \sqrt{\frac{C_p\, m^{\frac{1}{10}} I^{\frac{1}{2}} \epsilon_0^{\frac{2}{5}}}{12^{\frac{1}{5}}\pi^{\frac{3}{5}} B_r^{\frac{3}{10}} e^{\frac{7}{10}} K^{\frac{7}{5}}}} = I^{\frac{1}{4}}\left(\frac{C_p^{10} m \epsilon_0^4}{B_r^3 12^2 \pi^6 e^7 K^{14}}\right)^{\frac{1}{20}} \approx 16\frac{I^{\frac{1}{4}}}{B_r^{\frac{3}{20}}} \tag{26}$$

Here, the fundamental physical and statistical constants can be approximated by a numerical value of 16 in standard units. For $I = 10$ nA, $B_r = 10^8$ $\text{Am}^{-2}\text{rad}^{-2}\text{V}^{-1}$, we obtain $\theta \gg 10$ mrad. In the diffraction limit, using $I = 10^{-18}B_r$, $\theta \gg 5 \times 10^{-4}B_r^{\frac{1}{10}} = 3$ mrad.

Moreover, for $B_r = 10^8\text{Am}^{-2}\text{rad}^{-2}\text{V}^{-1}$, we find $B_r^{\frac{3}{20}} = 16$. Assuming that reduced brightness of modern SEM sources varies within a factor of 10 of this value, the result for $B_r^{\frac{3}{20}}$ will differ by no more than a factor of $10^{\frac{3}{20}} \approx 1.4$, which can be considered negligible for typical scaling purposes. Therefore, one may generally assume the requirement $\theta \gg I^{\frac{1}{4}}$ in standard units, using the pencil-beam approximation. Although $\theta \gg 10$ mrad may pose engineering challenges, it does not represent an intrinsic limitation of monochromator design.

To explore what really limits the practical performance of a monochromator, we now examine the tolerances. We begin with the deflection potential tolerances. The relative tolerance of the power supply can be obtained by requiring that $d\phi_s \ll d\phi_{\alpha,\text{Co,B}}$.

As an example, assuming $L = 0.02$m,[5] this yields

$$\frac{\delta\phi}{\Delta\phi} \ll \frac{2I}{\phi}\left[\left(\frac{Km}{\epsilon_0 e^2}\right)^2\left(\frac{12}{B_r\pi^2}\right)\right]^{\frac{1}{5}} = \frac{2}{L}\left(\frac{12}{B_r\pi^2}\right)^{\frac{2}{5}}\left(\frac{\epsilon_0 e^2}{Km}\right)^{\frac{1}{5}} \approx 6 \times 10^{-6}. \tag{27}$$

This tolerance is still achievable for LVSEM equipped with a stable power supply (i.e., resolution significantly better than17.4 bits). For TEM, however, $\delta\phi$ is superimposed on the main acceleration potential. For example, for $D = 1$ mm and $\theta = 0.1$ rad, $\delta\phi$ becomes:

$$\delta\phi \ll \frac{\Delta\phi}{\phi} d\phi_{\alpha,\text{Co,B}} = \frac{4I\theta D}{L}\left[\left(\frac{Km}{\epsilon_0 e^2}\right)^2\left(\frac{12}{B_r\pi^2}\right)\right]^{\frac{1}{5}} \approx 8 \times 10^{-5}\ \text{V}. \tag{28}$$

Although maintaining this level of accuracy is possible in principle, stacking the deflection voltage supply on top of an acceleration potential of 100 kV requires a relative stability of $\ll 8 \times 10^{-10}$. This imposes a significant engineering challenge and explains the limited temporal stability, typically in the millisecond range [9,14].

To determine the mechanical alignment tolerances, we require $d\phi_\varphi \ll d\phi_{\alpha,\text{Co,B}}$ which yields

$$\varphi \ll \frac{D\theta}{L^{\frac{3}{2}}}\left[\frac{12^7\epsilon_0 e^2}{B_r^2\pi^4 Km}\right]^{\frac{1}{10}} \approx 3 \times 10^{-5}\ \text{rad} \tag{29}$$

for the same illustrative values, this extremely low tolerance implies the need for additional stigmators and other correction elements to compensate for aberrations induced by misalignments. Therefore, in designing a new type of monochromator, the tolerances of both the electronics and mechanical components should be a primary focus.

4. Simple electrostatic monochromator approach

Monochromators such as those described in Section 1 inherently suffer from the limitation discussed in Section 2 and 3. To circumvent these issues, conventional monochromators rely on additional complex correction elements and supporting electronics. In this section, we present a new approach for a simplified monochromator design. Compared with conventional high- performance monochromators, the complexity is significantly reduced, while the performance remains unaffected.

4.1. Electrostatic fringe field deflectors

Eqs. (12) and (14) show that the electro-mechanical tolerances scale inversely with D. This parameter can therefore be tuned to achieve an improved design. For an electrostatic deflector, if $D \approx L$, the fringe field becomes important and needs to be included in the calculation of θ. When $D \gg L$, the fringe field contributions dominate the shape of the potential, hence the name "fringe-field deflector". To model the fringe-field effect, the potential is approximated by two line charges, adapted from [15]:

[5] The validity of these numbers is discussed in Appendix 1. In practice, the deflection angles and the deflector length can be larger, but this requires deviation from a straight path through a homogenous deflection field. Although the terms that are analysed here still contribute under such circumstances, higher order terms start to become more important, and should be considered as part of a detailed particular design. We aim to limit ourselves to the inherent effects of an uncorrected ideal deflector here. However, as can be seen in equation 29, increasing θ beyond the point where the thin, homogeneous deflector model works well to completely describe the optics, should increase the alignment tolerances.

$$\phi = \phi_0 + \frac{\Delta\phi}{4}\ln\frac{\sqrt{\left(x+\frac{D}{2}\right)^2+z^2}}{\sqrt{\left(x-\frac{D}{2}\right)^2+z^2}} \tag{30}$$

$$= \phi_0 + \frac{\Delta\phi}{8}\ln\frac{\left(x+\frac{D}{2}\right)^2+z^2}{\left(x-\frac{D}{2}\right)^2+z^2}, \tag{31}$$

Here, $\Delta\phi$ and D are chosen such that the electric field strength at the centre of the deflector is the same[6] as that of a homogeneous deflector. Applying the same mathematical procedure as described in subSection 2.1 now requires calculating the higher-order derivatives around $\phi(x = 0)$. Taking these higher-order derivatives of Eq. (30) with respect to x and evaluating them at $x = 0$ results:

$$\phi(0) = \phi_0 \tag{32}$$

$$\phi'(0) = \Delta\phi\frac{D}{D^2+4z^2} \tag{33}$$

$$\phi''(0) = 0 \tag{34}$$

$$\phi'''(0) = \Delta\phi\frac{8D\left(D^2-12z^2\right)}{\left(D^2+4z^2\right)^3} \tag{35}$$

Substituting these derivatives in Eq. (7) and integrating over z from $-\infty$ to ∞ yields

$$\theta_f = \theta_{f,0} - \frac{x}{D}\frac{\theta_{f,0}^2}{\pi} + \left(\frac{x}{D}\right)^2\frac{9\theta_{f,0}^3}{4\pi^2} \tag{36}$$

Here, the nominal deflection angle $\theta_{f,0} = \frac{\pi\Delta\phi}{4\phi_0}$, which is no longer dependent on D, thereby eliminating the first-order misalignment effects that contribute to $d\phi_\varphi$.

The contribution $d\phi_s$ in Eq. (24) remains unchanged when transitioning from homogeneous to fringe-field deflection. However, for homogeneous deflection fields $d\phi_s = \frac{\phi}{\Delta\phi}\delta\phi = \frac{L}{2D\theta}\delta\phi$, whereas for fringe-fields $d\phi_s = \frac{\pi}{4\theta}\delta\phi$. This indicates a difference in sensitivity to $\delta\phi$, with a ratio of $\frac{2L}{\pi D}$. Therefore, a deflector dominated by a homogeneous field, particularly when the deflector length L is much greater than the gap D, is more sensitive to $\delta\phi$, which is generally undesirable.

In contrast, fringe-field-dominated configurations can ideally achieve $d\phi_s \approx \delta\phi$, resulting in minimal sensitivity to angular deviations. This configuration is preferable, provided that the required energy dispersion $\Delta\phi$ can still be achieved without triggering a electrical breakdown. Although further improvements may be possible, in practice the drift of the acceleration potential in a TEM becomes the dominant source of error, since it typically scales as $d\phi_s \approx \delta\phi$. In the case of LVSEM, however, this particular limitation may not apply. Nevertheless, in practical implementations, there is often a residual contribution to $d\phi_s$, that scales as $d\phi_s \geq \delta\phi$.

For the potential described in [15] for finite cylinders, the parameter $\frac{D}{2}$ in Eq. (36) is replaced by $\sqrt{d^2-a^2}$, where d is half the distance between the centres of the cylinders, and a is the radius of the cylinders. This substitution does not alter any of the conclusions previously drawn for the line-charges model. However, the factor $\Delta\phi/4$ is replaced by $\frac{1}{2}\Delta\phi g$, where

$$g := \frac{1}{\ln\left(\hat{d}+\sqrt{\hat{d}^2-1}\right)} \tag{37}$$

and $\hat{d} := d/a$. This introduces a new sensitivity to rotational misalignments in the final result. To analyse the relative sensitivity of g, we compute

$$\frac{\partial g}{\partial\hat{d}}\frac{\hat{d}}{g} = \frac{\hat{d}}{\sqrt{\hat{d}^2-1}\ln\left(\hat{d}+\sqrt{\hat{d}^2-1}\right)} \tag{38}$$

Although this yields a finite tilt sensitivity, it converges to zero for $\hat{d} \gg 1$, where the line-charge approximation is recovered.

4.2. Beam energy variation

As discussed in subsection 0, $d\phi_\varphi$ can be neglected for fringe-field configurations. We assume $\Delta\phi \approx \phi_0$ to minimize $d\phi_s$, which gives a larger deflection angle $\theta_{f,0} \approx \frac{\pi}{4}$, leading to $d\phi_s \approx \delta\phi$. Finally, for typical probe currents applicable in an SEM, $\theta_{f,0} \approx \frac{\pi}{4} \gg I^{\frac{1}{4}}$ implies that trajectory displacement can be neglected. the remaining contributions are therefore

$$d\phi_{\text{tot}} = d\phi_{\alpha,\text{Co,B}} + d\phi_s \tag{39}$$

$$= 2I\left[\left(\frac{Km}{\epsilon_0 e^2}\right)^2\left(\frac{12}{B_r\pi^2}\right)\right]^{\frac{1}{5}} + \delta\phi \tag{40}$$

The value of $d\phi_{\alpha,\text{Co,B}}$ is retained from the homogeneous-field case. Although the results for $d\phi_{Co}$ differ by a factor $\frac{3/2}{9/4\pi^2}$ between the fringe-field and homogeneous-field configuration when $D = L$, only the scaling behaviour of the final result is considered. The numerical prefactor of $d\phi_{Co}$ appears with a power $\frac{1}{5}$ in the final expression and is therefore relatively insignificant. The goal here is not to obtain an exact numerical constant, but rather to establish a general scaling law. To arrive at this conclusion, we assume $L \approx D$, which determines ϕ according to Eq. (22). Assuming a practical configuration with $D = L = 2$ mm limited by both the vacuum pump budget and the difficulty of controlling electrostatic fields near the vacuum chamber walls for larger geometries, the optimal potential is $\phi = 85$ V, which is much lower than any typical voltages used in the electron gun region. Moreover, increasing the size or beam energy would raise the deflection voltages, which become difficult to place it into the microscope once they exceed ≈ 1 kV, as this risks electrical discharges. It is important to note that this value represents the optimal beam energy within the deflection space only. To minimize Boersch broadening, this low beam energy should also be restricted to the deflection region itself.[7] Although this is technically feasible, it implies that the entry and exit regions of the deflection space effectively act as lenses with short focal lengths. To minimize the geometric aberrations of these deceleration and acceleration lenses, they should be designed to have comparable physical dimensions. If made too small, the spherical aberrations of these lenses will dominate the energy resolution; if made too large, the deflectors fields will strongly influence the deceleration and acceleration lens fields, introducing large astigmatism that would require additional correction elements. An optimal balance among all factors contributing to $d\phi$ can therefore be achieved by designing a monochromator entirely based on fringe fields, in which

[6] Any other amplitude results in a different $\theta_{f,0}$, but the scaling as a function of $\theta_{f,0}$ remains the same.

[7] This approach is partially realized in [16], where the beam is decelerated before deflection. However, this configuration can be improved since the beam drifts at the same energy before reaching the selection aperture, creating unnecessary drift space at low beam energy, adding susceptibility to Boersch broadening and stray field interference.

the fields of the dispersive deflector (s) and the transfer lenses overlap. Such a configuration can be realized by stacking small, precisely aligned electrodes fabricated using Micro-fabrication (MEMS) techniques. In this design, the fringe fields of the deflector electrodes, deceleration and acceleration lenses have comparable spatial dimensions and should therefore be modelled collectively, taking their mutual interactions into account. Due to the typical voltages and electric fields achievable in such a MEMS-based monochromator, the deflection field should be positioned before the main acceleration potential in systems such as (S) TEM's.

5. Conclusion

Electrostatic or magnetostatic deflection fields serve as the main dispersion elements in current monochromator designs. Using a thin-deflector model, we have shown that the intrinsic energy resolution of a monochromator is fundamentally independent of its geometric dimensions, provided that the beam parameters are properly scaled. In the diffraction limit, this yields an achievable energy resolution on the order of 0.1 meV.

For homogeneous deflection fields, however, the required mechanical alignment tolerances are extremely stringent ($\ll 3 \times 10^{-5}$ rad), exceeding what is reliably achievable with current fabrication technologies. To suppress parasitic aberrations, modern monochromators therefore rely on additional multipole-based correction elements. These elements demand precise tuning of multiple power supplies, which increases system complexity, reduces practical energy resolution, and raises cost. We show that these tight mechanical-tolerance constraints can be greatly relaxed by adopting a fringe-field-dominated deflector design, which simultaneously reduces sensitivity to power-supply instabilities. The optimum beam energy resolution is obtained when the beam is decelerated locally immediately before the dispersion deflector, minimizing Boersch broadening. The compact geometry of a fringe-field deflector, combined with the short-range decelerating and accelerating fields that surround it, makes MEMS-based fabrication particularly attractive. To the best of our knowledge, a fully electrostatic MEMS monochromator of this type has not yet been realized. We acknowledge that industrial groups may have developed internal scaling laws similar to those presented here, or tailored to specific designs. However, we are unaware of any publicly available general design criteria of the form derived in this work.

CRediT authorship contribution statement

M.J. Adriaans: Writing – review & editing, Writing – original draft, Methodology, Investigation, Formal analysis, Conceptualization. **J.P. Hoogenboom:** Resources, Project administration, Funding acquisition. **A. Mohammadi-Gheidari:** Writing – review & editing, Supervision, Resources, Project administration, Funding acquisition.

Declaration of competing interest

The authors declare the following financial interests/personal relationships which may be considered as potential competing interests: Martijn Adriaans reports financial support was provided by Delft University of Technology. Martijn Adriaans reports a relationship with Delft University of Technology that includes: employment. Martijn Adriaans has patent pending to Delft University of Technology. If there are other authors, they declare that they have no known competing financial interests or personal relationships that could have appeared to influence the work reported in this paper.

Appendix

Parabolic trajectory and dimensions of a homogeneous deflector

For a homogeneous deflection field, instead of assuming any trajectory for the electron in a deflector, since

$$\phi = \phi_0 + \frac{\Delta\phi}{D}x \tag{41}$$

we have $\frac{dv_{z,1}}{dt} = 0$ inside the deflection field. However, it is different from $v_{z,0}$ outside the deflector because of the acceleration at the boundaries of the deflector. Assuming a sharp cut-off between the $\phi = \phi_0$ outside the deflector and inside (Eq. (41)) the deflector, the electron experiences an instantaneous acceleration in the z-direction such that by conservation of energy, the z-velocity inside the deflector $v_{z,1}$ (through conservation of energy) is given by

$$\frac{1}{2}mv_1^2 = \frac{1}{2}m\left(v_{z,1}^2 + {v_{x,1}}^2\right) = e\phi \tag{42}$$

$$v_{z,1} = \sqrt{\frac{2}{m}}\sqrt{e\phi_0 + \frac{e\Delta\phi}{D}x - \frac{1}{2}mv_{x,1}^2} \tag{43}$$

Assuming symmetric deflection, the x-velocity before and immediately after entering the deflector respectively $v_{x,0} = v_{x,1} = \frac{1}{2}\Delta v_x$. Then, a constant electrostatic force in the x-direction over a time interval $\Delta t = \frac{L}{v_{z,1}}$ with substitution of Eq. (43) yields

$$\Delta \mathrm{v_x} = \frac{e\Delta\phi}{mD}\frac{L}{v_{z,1}} = \frac{e\Delta\phi L}{mD}\frac{1}{\sqrt{\frac{2}{m}}\sqrt{e\phi_0 + \frac{e\Delta\phi}{D}x - \frac{1}{8}m\Delta v_x^2}} \tag{44}$$

Then, by dividing by v_0 to get $\widetilde{\theta} := \frac{\Delta \mathrm{v_x}}{v_0} = 2\sin\frac{\theta}{2}$, where $v_0 = \sqrt{\frac{2e\phi_0}{m}}$ this simplifies to

$$\widetilde{\theta} = \frac{\theta_0}{\sqrt{1 + 2\theta_0 x - \frac{1}{4}\widetilde{\theta}^2}}, \tag{45}$$

where $\mathrm{x} := \frac{x}{L}$ and again $\theta_0 := \frac{L\Delta\phi}{2D\phi_0}$. Squaring both sides and solving for $\widetilde{\theta}^2$ we get

$$\widetilde{\theta}^2 = 2(1+2\theta_0 x) \pm 2\sqrt{(1+2\theta_0 x)^2 - \theta_0^2}, \tag{46}$$

where subtraction of the two terms represent the physical result since then $\widetilde{\theta}(\theta_0 = 0) = 0$.

Then, taking the square root and of this result we get

$$\widetilde{\theta} = \sqrt{2(1+2\theta_0 x) - 2\sqrt{(1+2\theta_0 x)^2 - \theta_0^2}}, \tag{47}$$

where we can finally retrieve θ as

$$\theta = 2\arcsin\frac{1}{2}\widetilde{\theta} = 2\arcsin\left(\frac{1}{2}\sqrt{2(1+2\theta_0 x) - 2\sqrt{(1+2\theta_0 x)^2 - \theta_0^2}}\right) \tag{48}$$

And then expanding the lowest order terms around $\theta_0 = 0,\ x = 0$ we retrieve

$$\theta \approx \theta_0 - x\theta_0^2 + \frac{3}{2}x^2\theta_0^3, \tag{49}$$

which is exactly the same as Eq. (10). From this we can deduce that setting $ds = dz$ results in the correct small angle deflection.

One might wonder what still counts as a "small" angle here. In this paper we care about the general scaling of the problem, instead of retrieving a result that is exact within a small percentage. Therefore, as long as the result so as long as the result does not diverge or more than double in magnitude past some point, it is considered accurate in scaling.

This can be tested by considering the expression θ around $x = 0$. In this case, Eq. (48) collapses to $\theta = \arcsin\theta_0$ (this can be derived by temporary substitution $\theta_0 = \cos\psi$, allowing the expression to collapse). Though this result for θ does not diverge to multiple times θ_0 within its entire range of definition, there is still a problem. In Eq. (2), the fraction $\frac{d\theta}{\theta}$ is implicitly approximated as $\frac{d\theta_{-0}}{\theta_{-0}}$ which results in the expression given. In this approximation, a derivative $\frac{d\theta}{d\theta_0}$ is implied to be neglected. The derivative $\frac{d\theta}{d\theta_0} = \frac{1}{\sqrt{1-\theta_0^2}}$ does actually diverge at $\theta_0 = 1$. Thus there is a largest angle at which the approximation of $\theta \approx \theta_0$ and thus $\frac{\left(\frac{d\theta}{d\theta_0}\right)d\theta}{\theta} \approx \frac{d\theta_0}{\theta_0}$ no longer holds. Assuming we want the result to be accurate within a factor 2, we can calculate the ratio a between the full result and the numerical approximation as

$$\frac{\left(\frac{\left[\frac{1}{\sqrt{1-\theta_0^2}}\right]}{\arcsin\theta_0}\right)}{\left(\frac{1}{\theta_0}\right)} = \frac{\theta_0}{\arcsin\theta_0\sqrt{1-\theta_0^2}} = a \tag{50}$$

Assuming we want the chromatic expression to be accurate within a factor of $a < 2$, this inequality can be numerically solved to yield a maximum $\theta_0 = 0.92$. As long as this is the case, the deflector is considered "thin" for the approximations in this paper to be considered valid.

Of course, this assumes that the beam actually fits through the width of the deflector at this angle. To make sure how much the beam curves throughout the deflector, we integrate the force in the x direction:

$$m\frac{d^2x}{dt^2} = e\frac{d\phi}{dx} = e\frac{\Delta\phi}{D} \tag{51}$$

leading the width of the trajectory in the x-direction Δx throughout the deflector

$$\frac{m}{e}\Delta x = \frac{1}{2}\frac{\Delta\phi}{D}(\Delta t/2)^2, \tag{52}$$

where $\Delta t = \frac{L}{v_{z,1}}$ is again the time it takes to traverse the whole deflector. Since the trajectory is assumed symmetrically through the deflector, the beam bends back after half the length of the deflector, hence a time $\frac{\Delta t}{2}$ until halfway the deflector. Though the rays generally accelerate or decelerate in the z-direction when passing the edges of the delfection field, the central ray (which enters at $x = 0$) does not. This means that for the central ray component, around $x(t = 0) = 0$, the velocity component $v_{z,1} = v_0\cos\frac{\theta}{2} = \sqrt{\frac{2e\phi_0}{m}}\cos\frac{\theta}{2}$ throughout the deflector. Therefore, substituting Δt and then $v_{z,1}$ yields

$$\Delta x = \frac{1}{16}\frac{\Delta\phi L^2}{D\phi_0}\frac{1}{\cos^2\frac{\theta}{2}}\ . \tag{53}$$

Though there is a $\cos\frac{\theta}{2}$ dependency, for small angles (even at $\theta = \arcsin 0.919$, the difference is "only" 43 %), this can be neglected. Furthermore, recognising once more the contribution $\theta_0 := \frac{L\Delta\phi}{2D\phi_0}$ yields

$$\Delta x = \frac{1}{8}\theta_0 L\ . \tag{54}$$

It should be noted that though this is the trajectory for the central ray only, it gives an estimate of the maximum offset of a ray passing through the

centre of the deflector, thus D should be at least twice this amount in case the beam passes through the centre of the deflector. In order to allow the beam to enter and exit at the center of a deflector, the width should thus be

$$D > 2\Delta x = \frac{1}{4}\theta_0 L. \tag{55}$$

In practice, depending on the more detailed design, the beam would not necessarily have to enter through the geometric centre of the deflector, since it just makes the symmetry of the calculation simpler.

Another reason that the beam might through the deflector is the radius of the beam itself.

The beam radius through the deflector can be computed from the brightness with $r = \sqrt{\frac{I}{B_r \pi^2 \alpha^2 \phi}}$, where substitution of Eqs. (20) and then 22 yield

$$r = \left(\frac{\left(\frac{2}{3}\right)^{\frac{2}{3}} I^{\frac{1}{3}}}{B_r^{\frac{1}{3}} \pi^{\frac{2}{3}} \phi^{\frac{1}{3}} \theta^2} \right)^{\frac{1}{2}} = \frac{2^{\frac{2}{5}} L^{\frac{1}{2}}}{3^{\frac{3}{10}} \pi^{\frac{2}{5}} B_r^{\frac{1}{5}} \left(\frac{Km}{\epsilon_0 e^2}\right)^{\frac{1}{10}} \theta}. \tag{56}$$

Since width of the beam is twice equal to the radius, the total width of the deflector should be $D > 2r + 2\Delta x$. With the example of $L = 0.02$ m and $\theta = 0.1$ rad as mentioned in the text, $2\Delta x \approx 0.1$ mm and $2r \approx 0.2$ mm. Therefore, $D = 1$ mm is wide enough to allow the beam to pass.

Data availability

Data will be made available on request.

References

[1] L. Liberman, O. Kleinerman, I. Davidovich, Y. Talmon, Micrograph contrast in low-voltage SEM and cryo-SEM, Ultramicroscopy. 218 (2020) 113085, https://doi.org/10.1016/j.ultramic.2020.113085. Nov.

[2] M.T. Postek, A.E. Vladár, D.L. Poster, A. Muto, T. Sunaoshi, Ultra-low landing energy scanning electron microscopy for nanoengineering applications and metrology, in: W. Park, A.-J. Attias, B. Panchapakesan (Eds.), Nanoengineering: Fabrication, Properties, Optics, Thin Films, and Devices XVII, SPIE, Online Only, United States, 2020, p. 25, https://doi.org/10.1117/12.2567051. Aug.

[3] A. Mohammadi-Gheidari, P. Kruit, Electron optics of multi-beam scanning electron microscope, Nucl. Instrum. Methods A 645 (1) (2011) 60.

[4] P. Tiemeijer, M. Bischoff, B. Freitag, C. Kisielowski, Using a monochromator to improve the resolution in TEM to below 0.5 Å Part I: creating highly coherent monochromated illumination, Ultramicroscopy. 114 (2012) 72–81.

[5] K. Kimoto, Practical aspects of monochromators developed for transmission electron microscopy, Microscopy. 63 (5) (2014) 337–344, https://doi.org/10.1093/jmicro/dfu027. Oct.

[6] A. Henstra, J. Chmelik, T. Dingle, A. Mangnus, G.V. Veen, Versatile Monochromator Module for XHR SEM, Microsc. Microanal. 15 (S2) (2009) 168–169, https://doi.org/10.1017/S1431927609096147. Jul.

[7] J. Junji, Calculation for geometrical aberrations of a deflection system with a uniform electrostatic field, J. Electron. China 4 (3) (1987) 192–199, https://doi.org/10.1007/BF02778955. Jul.

[8] A. Mohammadi-Gheidari, P.C. Tiemeijer, A. Henstra, and T. Radlicka, Electron optical module for providing an off-axial electron beam with a tunable coma. (2023). US11804357B2.

[9] Terauchi, Tanaka, Tsuno, Ishida, Development of a high energy resolution electron energy-loss spectroscopy microscope, J. Microsc. 194 (1) (1999) 203–209, https://doi.org/10.1046/j.1365-2818.1999.00450.x. Apr.

[10] S. Lopatin, B. Cheng, W.-T. Liu, M.-L. Tsai, J.-H. He, A. Chuvilin, Optimization of monochromated TEM for ultimate resolution imaging and ultrahigh resolution electron energy loss spectroscopy, Ultramicroscopy. 184 (2018) 109–115, https://doi.org/10.1016/j.ultramic.2017.08.016. Jan.

[11] J. Orloff (Ed.), Handbook of Charged Particle Optics, 2nd ed., CRC Press/Taylor & Francis, Boca Raton, 2009.

[12] H. Ibach, H. Sato, M. Kubo, F.S. Tautz, H. Yoshida, F.C. Bocquet, A novel high-current, high-resolution, low-kinetic-energy electron source for inverse photoemission spectroscopy, Rev. Sci. Instrum. 94 (4) (2023) 043908, https://doi.org/10.1063/5.0138512. Apr.

[13] A. Mohammadi-Gheidari, 196 Electron Beams in an Scanning Electron Microscope, Delft University of Technology, Delft, 2013.

[14] E. Essers, et al., Energy resolution of an Omega-type monochromator and imaging properties of the MANDOLINE filter, Ultramicroscopy. 110 (8) (2010) 971–980, https://doi.org/10.1016/j.ultramic.2010.02.009. Jul.

[15] K. Engelen, P. Jacqmaer, J. Driesen, Electric and magnetic fields of two infinitely long parallel cylindrical conductors carrying a DC current, Eur. Phys. J. Appl. Phys. 64 (2) (2013) 24515, https://doi.org/10.1051/epjap/2013120441. Nov.

[16] H. Mook, P. Kruit, Construction and characterization of the fringe field monochromator for a field emission gun, Ultramicroscopy. 81 (3–4) (2000) 129–139.